We are IntechOpen, the world's leading publisher of Open Access books Built by scientists, for scientists

4,800
Open access books available

122,000
International authors and editors

135M
Downloads

Our authors are among the

154
Countries delivered to

TOP 1%
most cited scientists

12.2%
Contributors from top 500 universities

CLARIVATE ANALYTICS BOOK CITATION INDEX INDEXED

WEB OF SCIENCE™

Selection of our books indexed in the Book Citation Index in Web of Science™ Core Collection (BKCI)

Interested in publishing with us?
Contact book.department@intechopen.com

Numbers displayed above are based on latest data collected.
For more information visit www.intechopen.com

1

Monte Carlo Simulations in NDT

Frank Sukowski and Norman Uhlmann
Fraunhofer Institute for Integrated Circuits IIS, Development Center X-ray Technology (EZRT)
Germany

1. Introduction

X-ray techniques are commonly used in the fields of non-destructive testing (NDT) of industrial parts, material characterization, security and examination of various other specimens. The most used techniques for obtaining images are radioscopy for 2D and computed tomography (CT) for 3D imaging. Apart from these two imaging techniques, where X-ray radiation penetrates matter, other methods like refraction or fluorescence analysis can also be used to obtain information about objects and materials. The vast diversity of possible specimen and examination tasks makes the development of universal X-ray devices impossible. It rather is necessary to develop and optimize X-ray machines for a specific task or at least for a limited range of tasks. The most important parameters that can be derived from object geometry and material composition are the X-ray energy or spectrum, the dimensions, the examination geometries and the size of the detector. The task itself demands a certain image quality which depends also on the X-ray spectrum, the examination geometry and furthermore on the size of the X-ray source's focal spot and the resolution of the detector.
Monte-Carlo (MC) simulations are a powerful tool to optimize an X-ray machine and its key components. The most important components are the radiation source, e.g. an X-ray tube and the detector. MC particle physics simulation codes like EGS (Nelson et al., 1985) or GEANT (Agostinelli et al., 2003) can describe all interactions of particles with matter in an X-ray environment very well. Almost all effects can be derived from these particle physics processes. The MC codes are event based. Every single primary particle is generated and tracked along with all secondary particles until the energy of all particles drops below a certain threshold. The primaries are generated one after another, since no interactions between particles take place.
When simulating X-ray sources, in most cases X-ray tubes, the primary particles are electrons. The electron beam is parameterized by the electrons' kinetic energy and the intensity profile along the cross-section of the beam. When hitting the target, X-rays are generated by interaction of electrons with the medium. The relevant magnitudes for imaging are the X-ray energy spectrum and the effective optical focal spot size (Morneburg, 1995).
The most used imaging systems in the field of NDT are flat panel detectors. There are two basic types of detectors: Direct converting semiconductor detectors and indirect converting scintillation detectors. The type of particle interactions in the respective sensor layer determines the detection efficiency and effective spatial resolution. Interaction of X-rays in direct converting detectors produces electron-hole-pairs in the semiconductor materials. The free charge carriers drift to electrodes, where the current can be measured. MC simulations can

describe the X-ray absorption and scattering as well as the electron drift which leads to image blurring. Measuring X-rays with scintillation detectors works differently. X-rays interact in the scintillation layer and produce visible photons, which are detected in a CCD or CMOS chip. In addition to X-ray scattering and electron drift the diffusion of the visible photons in the scintillation layer contributes greatly to image blurring (Beutel et al., 2000). In any case, a thicker sensor layer improves the detection efficiency on the one hand, which leads to shorter measurement times, but decreases the spatial resolution on the other hand. Finding the optimal trade-off between efficiency and resolution by designing detector properties is an excellent task for MC simulations.

Another application field of MC simulations are feasibility studies for special examination tasks in order to evaluate physical limits of different imaging methods. These studies are not limited to radioscopic methods, but include other ways to obtain information about specimens like refractive, diffractive and backscatter imaging as well as fluorescence analysis and many more.

In this chapter MC applications aimed at the optimization of X-ray setups for specific tasks and feasibility studies are introduced.

The used Monte-Carlo code is called ROSI (ROentgen SImulation), which was developed by J. Giersch and A. Weidemann at the University of Erlangen (Giersch et al., 2003). Is is an object oriented programm code and the simulation runs can be parallelized in a computer network for largely increasing the performance. It is based on the particle physics codes EGS4 for general electromagnetic particle interactions and LSCAT for low energy processes.

2. Simulation of X-ray sources

2.1 X-ray source characteristics in NDT imaging

In common X-ray tubes, radiation is produced by accellerating electrons via a potential difference between the cathode (the electron emitter) and the anode (the X-ray target). When the electrons hit the target, they are decelerated hard by collisions with electrons of the target material or in the coulomb fields of atomic cores. X-ray radiation is produced in two different processes. Since electrons are charged, acceleration or in this case deceleration can cause emission of photons. The energy of these photons corresponds to the electrons' energy loss during the deceleration process, so the maximum possible energy corresponds to the acceleration voltage ($E_{\max} = e \cdot U$). This process is called bremsstrahlung. The other process is called characteristic or fluorescence radiation and takes place when electrons ionize the target material by hitting bound electrons. The excited atoms change into their ground state very quickly by electronic transition from a high to the lower vacant energy level. During this process a photon is emitted, whose energy corresponds to the difference in these energy levels (Morneburg, 1995).

2.1.1 Energy spectrum

In the field of X-ray imaging the kind of application forces all neccessary source properties. When penetration techniques like radiography or computed tomography are used, the X-ray radiation energy is one of the most important parameters. The radiation must partially penetrate the object to obtain the highest possible contrast between high and low absorbing parts of the specimen. With X-ray tubes as sources, the energy spectrum can be shaped by adjusting the tube voltage and using various prefilters. Figure 1 shows spectra between 30 and 450 kV with several prefilters.

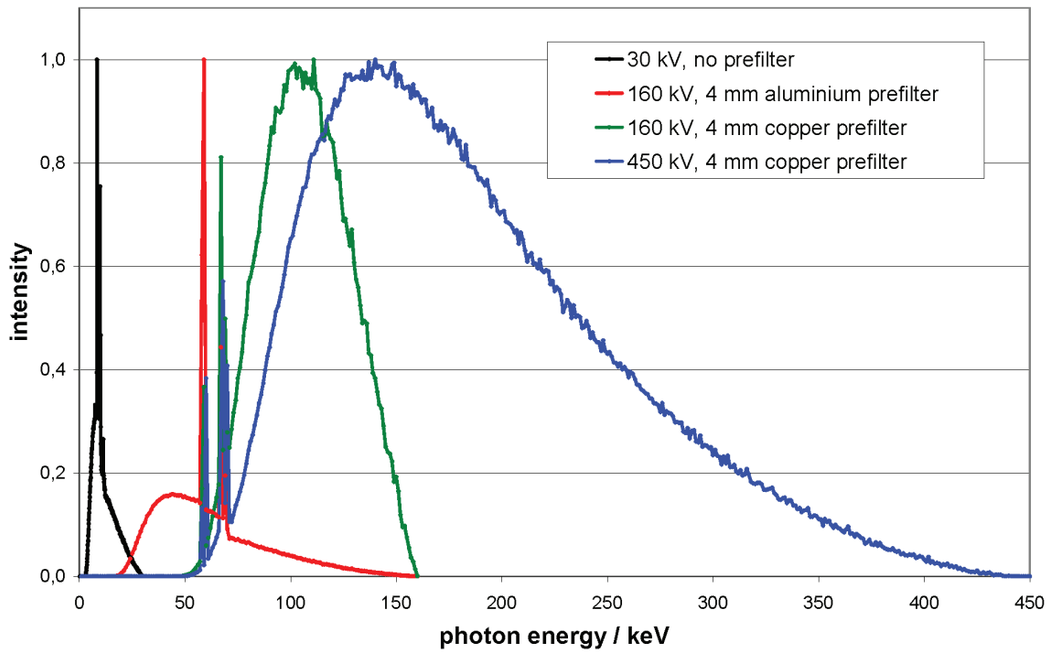

Fig. 1. X-ray spectra, normalized to a maximum of 1

The influence of the image quality can clearly be seen in 2. A Siemensstern with 8 mm thick iron and copper sections is radiographed. (a) The energy of the X-rays is not sufficient to penetrate any material, the area behind the object is completely dark. (b) The area behind the object is still very dark compared to the uncovered area, although a faint contrast between copper (darker) and iron (lighter) can be seen. Many low energy photons enhance the brightness in the uncovered area, while they are completely absorbed in the object. (c) The low-energy photons are filtered out by the prefilter and don't contribute to either the uncovered or covered image parts. The difference between these areas is reduced, while the contrast is enhanced. This spectrum would be a good choice for separating the iron and copper sections. (d) The vast majority of the photons penetrate the object regardless of the material. The complete object appears brighter, but the contrast between iron and copper is reduced again.

2.1.2 Focal spot size

The focal spot size U_F of the X-ray source is also a very important magnitude and has a large influence on the spatial resolution of the image, especially when working with high magnifications M. The magnification is given by the fraction of the focus-detector-distance FDD and the focus-object-distance FOD. As illustrated in 3, the geometrical unsharpness U_g of the image is given by

$$U_g = U_F\,(1 - M) = d\left(1 - \frac{FDD}{FOD}\right). \tag{1}$$

2.1.3 Intensity

With many applications, the measurement time is crucial and should be as short as possible. The image noise on one hand results from electronic noise in detector systems, but the main

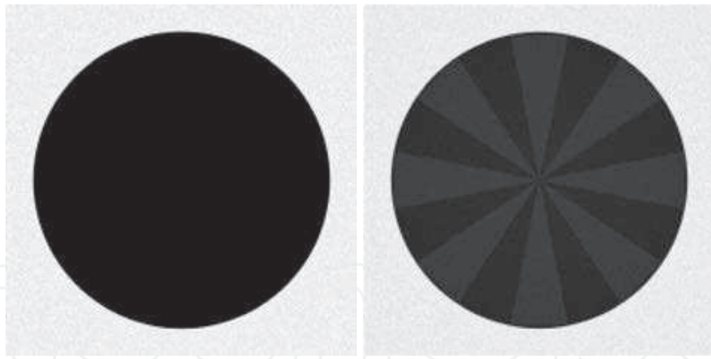

(a) 30 kV without prefilter (b) 160 kV with 4 mm aluminium prefilter

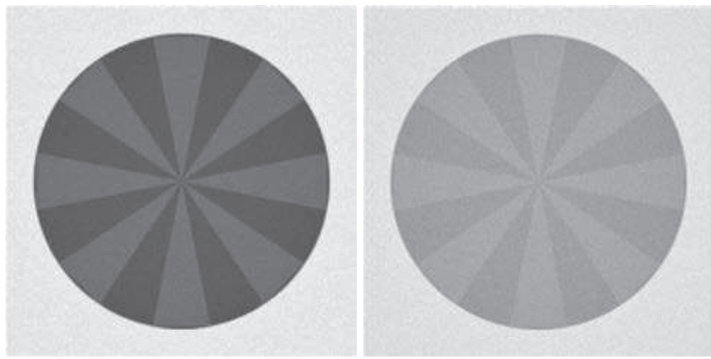

(c) 160 kV with 4 mm copper prefilter (d) 450 kV with 4 mm copper prefilter

Fig. 2. Images of a Siemensstern. The sections are iron and copper with thickness of 8 mm each

part originates from poisson noise due to limited quantum statistics. Poisson noise is $1/\sqrt{N_p}$, where N_p is the number of events per pixel in one image. For obtaining low-noise images in a short time, the source intensity must be maximized. The number of emitted photons from an X-ray source first depends on the tube voltage U. The intensity is roughly proportional to the squared voltage. Since the voltage shapes the energy spectrum, it is not always desirable to change it for a given application. The second way to increase the intensity is to increase the tube current I, which is proportional to the intensity. The electrical power P applied to the X-ray target is $P = U \cdot I$. Unfortunately only about 1% of the electrical power is converted to X-rays. The vast majority of the electrical power heats up the target, which forces a limitation in the appliable current. Monte-Carlo simulations can help a great deal to optimize target material composition and geometry to increase the load capacity of targets or increase the X-ray conversion efficiency.

2.2 High resolution imaging

As mentioned in the above section, a small focal spot is crucial to achieve a good spatial resolution when working with high magnifications. High resolution in X-ray imaging means resolution of object details below 1 micron. For those applications, microfocus X-ray tubes with transmission targets are commonly used where the target is also the exitation window of

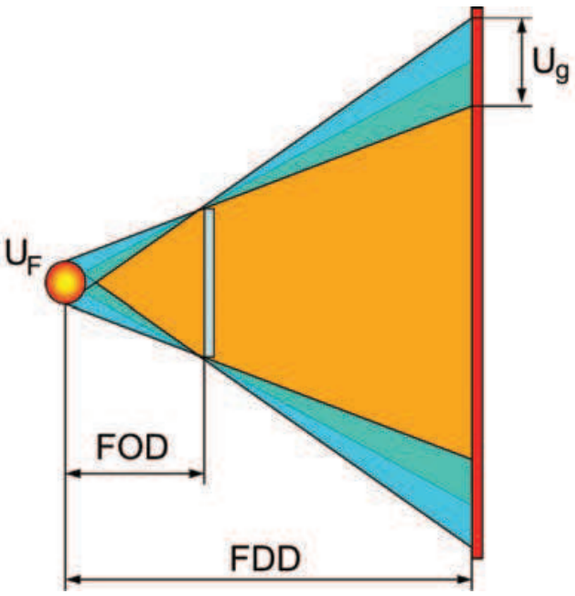

Fig. 3. Geometrical unsharpness due to X-ray source dimension

the tube. The transmission target has a great advantage since the specimen can be placed very close to the focal spot in order to achive high magnifications. The electron beam in the X-ray tube is focused onto the target by electronic lenses. The diamater of the beam on the target surface reaches from 200 nm to several μm and mostly determines the X-ray focal spot size. But the diffusion of the electrons in the target, which depends largely on the target materials and layer composition can further increase the focal spot size as shown in 4. To design a target for smallest possible focal spots, Monte-Carlo simulations of electronic diffusion and X-ray production processes were performed.

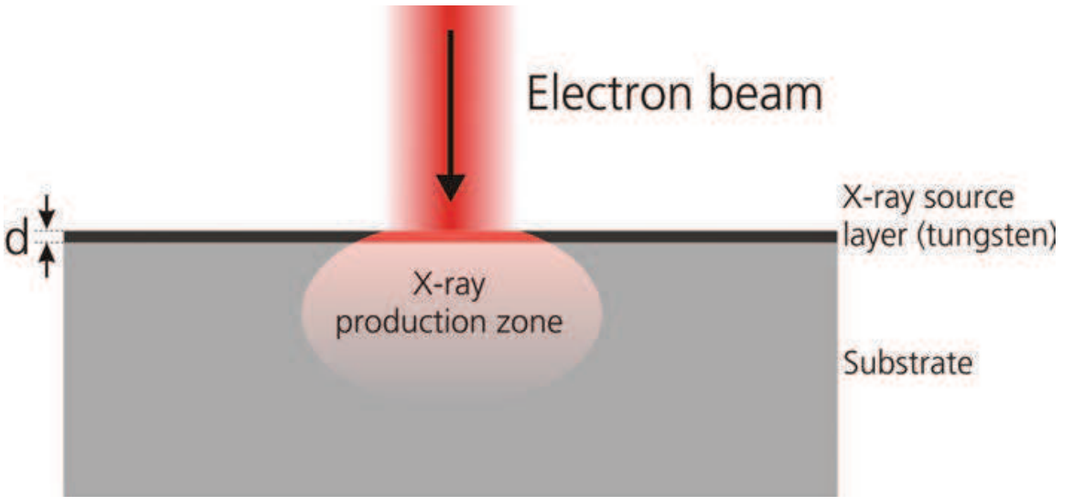

Fig. 4. Geometrical setup of a transmission target

In the simulation a parallel electron beam with electron kinetic energy between 30 and 120 keV was modeled with a gaussian intensity cross-section in both dimensions. The FWHM value of the gaussian distribution was 200 nm. The first layer material of the transmission target

is tungsten. Since the X-ray productivity rises with the atomic number proportional to Z^2, tungsten with $Z = 74$ is a good choice. It has even more advantages, a very high melting point at over 3000 °C, a fair thermal conductivity, mechanical and chemical stability. The X-rays are produced mainly in the tungsten layer, which is also called the X-ray production layer. In the simulations, the thickness of this layer was varied from 0.05 to 7 microns (depending on electron energy). From their point of origin the photons have to pass the remaining target material to reach the side opposite the electron beam. Therefore the substrate material must fulfill serveral requirements. The atomic number must be quite low, so the X-rays can pass that layer without being absorbed, even at low energies. Furthermore, the substrate must have a good thermal conductivity and a high melting point so that the heat that is generated in the tungsten layer can be conducted to the air side of the target, where it can be cooled by fans for example. A performance number can be approximated by the product of thermal conductivity λ and maximum allowable temperatur $T_{\max}$. A further task of the substrate is to form a mechanical closure of the vacuum vessel against the air pressure. Since the target must be thin for X-ray transmissibility, the material must be quite stable. Common materials for this task are beryllium, aluminium, diamond or other carbon configurations. The simulations were done for a 300 micron thick beryllium substrate, which forms a quite stable vaccum closure. As simulation results the diameter of the effective focal spot U_F, i.e. the area where photons are produced and the X-ray production efficiency were obtained. The total X-ray intensity ϕ and the brillance b, which is defined as the intensity divided by the source area are also important magnitudes for some applications.

$$b = \frac{\phi}{A_F} = \frac{4\phi}{\pi U_F^2} \tag{2}$$

Determining the focal spot size U_F from simulation data is shown in 5. The two-dimensional energy distribution of generated X-rays on the target was calculated with ROSI (a). The focal spot profile was taken from a line profile averaged over the whole target width in one direction (b). This profile was integrated after normalizing the total X-ray power to a value of 1. The focal spot is defined as the area where the integral value is between 0.1 and 0.9 (c).

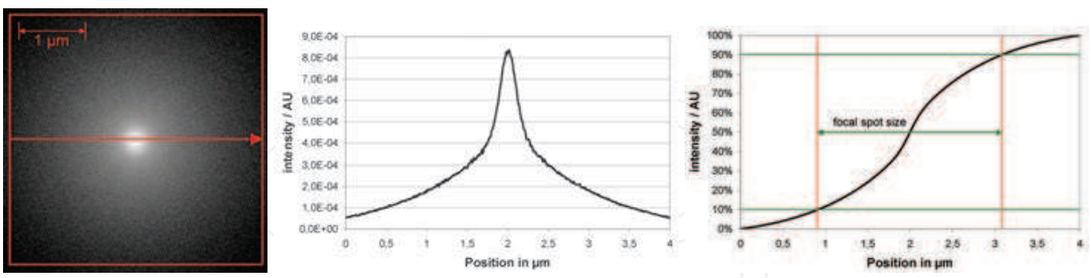

(a) X-ray energy distribution of all generation locations

(b) One-dimensional focal spot profile averaged over whole width

(c) Integral over normalized profile

Fig. 5. Determination of focal spot sizes

In figure 6 the effective focal spot size U_F (a), the X-ray intensity ϕ (b) and the brillance b (c) is shown for several tungsten layer thicknesses and the tube voltages of 30, 70 and 120 kV. The intensities are calculated per target current.
For each voltage, all curves follow a similar course. The focal spot size can never be smaller than the diameter of the electron beam, so it is nearly 200 microns in diameter with very thin

tungsten layers, since only a few electrons interact with that layer and are barely scattered to distant parts of the tungsten. Due to the small interaction probability, the X-ray intensity is also very low. With thicker tungsten layers, the interaction probability and therefore the production rate of photons rises rapidly. Since the average scattering angles are quite small, especially at higher voltages, the electron beam barely broadens in that layer, keeping the focal spot size almost constant. The brillance rises to a maximum until the tungsten becomes thick enough so that electrons can be scattered multiply, reaching distant parts of that layer, where they also produce X-rays. The result is an increase of the focal spot size. The total number of photons produced and reaching the opposite side of the target still rises until the tungsten becomes so thick, that the photons are reabsorbed by the tungsten. The focal spot size gets into saturation and the intensity is again reduced by higher target self-absorption.

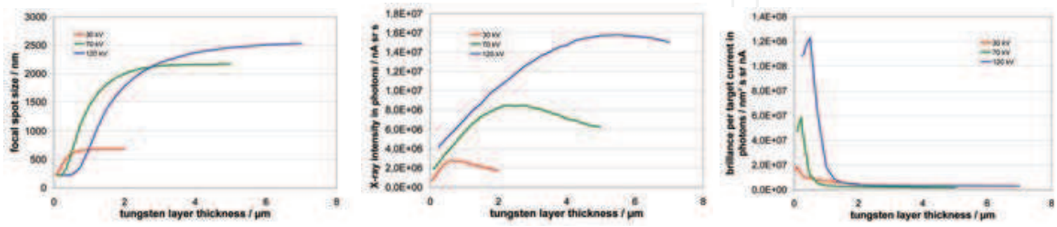

(a) Focal spot size (b) X-ray intensity (c) Source brillance

Fig. 6. Optimization of target configuration with nano focus sources

Of course the simulations can also be done with other substrate materials and thicknesses to find optimal parameters for a specific application. The Monte Carlo simulation can also calculate the heat deposition in the target volume. The data can then be taken into a heat transfer simulation tool to calculate the heat load capacity of the whole target.

2.3 High energy imaging

Imaging of very large and dense objects such as freight containers, whole cars (especially engines) or parts from shipbuilding requires very high energetic radiation in the MeV range to penetrate these objects. X-ray tubes on the market are available up to voltages of 450 kV, which is by far not enough. To produce high energy X-rays linear accelerators (LINACs) are commonly used. The principle in generating X-rays is the same, but the method of accelerating the electrons differs from X-ray tubes. The electrons are emitted by a gun and accelerated by bundles in a waveguide through several copper cavities. A high voltage microwave signal is applied, which accelerates the electron bundles over several cavities up to kinetic energies of some MeVs.

When electrons hit the target at these energies, X-ray radiation is almost solely produced in the direction of the impacting electrons, so X-ray targets work exclusively as transmission targets. The relativistic Lamor formula describes the angular distribution of bremsstrahlung generation (Jackson, 2006):

$$\frac{\mathrm{d}P}{\mathrm{d}\Omega} = \frac{e^2\dot{v}^2}{4\pi c^3}\frac{\sin^2\theta}{(1-\beta\cos\theta)^5} \tag{3}$$

At very high energies and small angles, $\beta = v/c \approx 1$, the denominator decreases with a power of five and the whole term gets very large. Using high energy X-rays for imaging means that the radiation field is limited or at least decreases rapidly in intensity at the borders. To

choose appropriate radiation geometries for different object sizes, the radiation field has to be calculated and taken into account.
We modeled a commonly X-ray target made of 800 μm copper and 450 μm tungsten. The electron beam was modeled as a parallel and monoenergetic beam. The intensity cross-section was gaussian in shape with a FWHM value of 1 mm. We calculated the angular X-ray intensity distribution for energies from 1 to 18 MeV (see 7).

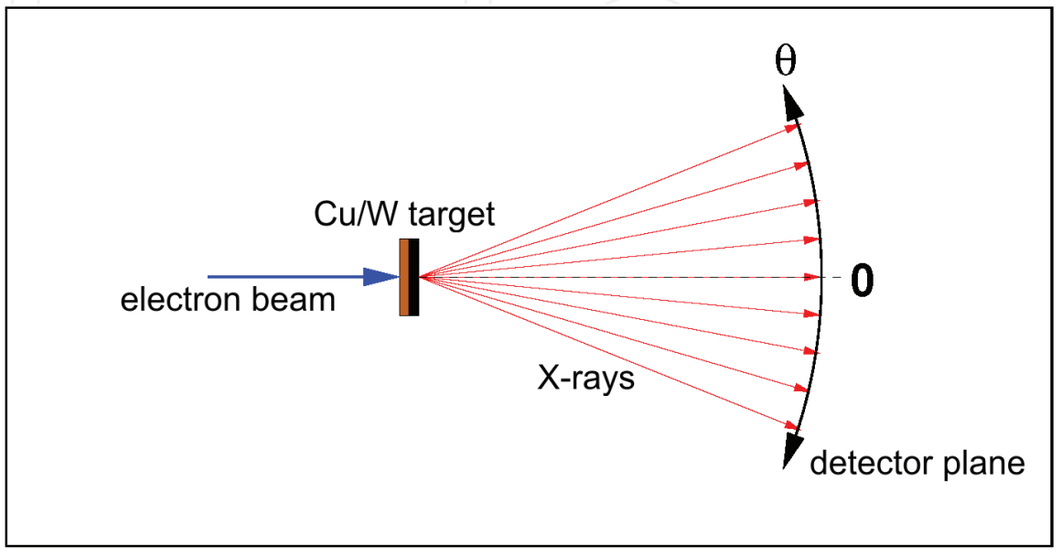

Fig. 7. Simulation setup for X-ray generation with a LINAC target

The results are shown in 8. The theoretically calculated distribution looks quite different to the simulation results. The Lamor formula assumes all electrons travelling in the forward direction ($\theta = 0°$) when generating bremsstrahlung. In reality the electrons can be scattered by collisions with other electrons and atomic cores while changing their direction before generating bremsstrahlung. The forward peak is blurred to higher angles. The absolute intensity increase with electron kinetic energy is described very well and corresponds to the theory.

2.4 Efficiency optimization

Some applications get along without high resolution or high energy sources. Sometimes a short measurement time is most essential. Inspection systems within an industrial production line have to measure prefabricated parts within a production cycle. When inspecting parts with computed tomography for reconstructing the whole 3-dimensional volume, this task is quite demanding, since the parts must be radiographed from several hundred points of view in a short time. The most important component to achieve this is a highly intense radiation source, that works normally with moderate voltages between 80 to 225 kV. Most X-ray tubes have fixed targets, where the electron beam hits the same spot on the target the whole time. The electron beam current is therefore limited due to heating up this focal spot. For medical X-ray imaging, there are tubes with rotating targets since 1933. The electron beam hits the target not in a single spot, but in a circular path. The load with rotating targets can be enhanced by a factor of approximately ten compared to fixed targets. The reasons why rotating targets are not common in industrial X-ray imaging are locally unstable and quite big focal spots of

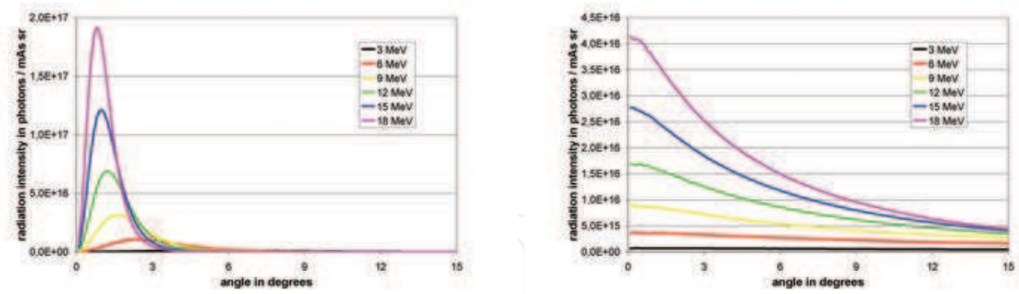

(a) Calculated with Lamor formula (b) Simulated with ROSI

Fig. 8. Analytically calculated and simulated angle distrubutions for generated X-rays in a LINAC target at high energies

about 800 microns or more and their very high price. They only are used where measurement time is crucial.
With Monte-Carlo simulations some work was done to improve the allowed target load by modifying both the electron beam geometry and target composition with rotating anodes (Sukowski, 2007). This work was done with a medical X-ray tube, but since industrial X-ray tubes are derived from medical tubes, the results can be conveyed to industral tubes without difficulty. Under variation of the tungsten layer thickness, the emitted X-ray intensity and energy deposition in the target was simulated. The 3-dimensional energy distribution can be transferred to finite element simulation programs to calculate the temperature distribution in steady state while taking cooling effects into account. With the simulation results, optimizing the electron beam and target geometries is possible.

3. Simulation of X-ray detectors

3.1 Types of detectors commonly used in NDT

In almost all X-ray imaging applications, line or area pixel sensors are used. An X-ray image is virtually the spatial distribution of the X-ray radiation intensity hitting the sensor area. When X-rays interact with the sensor material, energy is transferred to the sensor and converted into an electrical signal. The signals are amplified and digitized pixel by pixel to a numeric value. The spatial pixel value distribution can be visualized by a color or more often used grey brightness scale. In a positive X-ray image, bright areas correspond to high X-ray intensity, where almost no material is between the X-ray source and the detector, while dark areas are usually covered by thick or heavy parts of the specimen (see 2). In the simulation studies we focused on characterizing flat-panel pixel detectors with squared or rectangular surfaces, which are the most used detectors. Basically there are two types of flat-panel detector technologies that differ in the way of conversion from X-ray energy deposition to an electrical signal (Beutel et al., 2000).

3.1.1 Indirect converting detectors

Most flat-panel detectors convert the X-ray energy deposition in an indirect way into an electrical signal. The X-ray detection mechanism is based on a scintillator. X-rays interacting with a scintillator ionize the atoms, causing emission of fluorescence light due to exited-state

deactivation. The energy level differences of some elements in a typical scintillator are in the range of some electronvolts. The fluorescence light emitted from the scintillator is therefore visual light that can be detected by a photo diode array which is arranged just behind the scintillator layer (Beutel et al., 2000).

3.1.2 Direct converting detectors

Unlike scintillator based detectors, direct converting detectors usually consist of a semiconductor material as sensor layer. The semiconductor is assembled between two electrodes. One electrode is continuous over the whole sensor area, while the other electrode on the opposite side consists of many small solder beads which resemble the detector pixels. Between the two electrodes a voltage is applied so that the semiconductor is completely depleted of charge carriers. When X-rays interact with the semiconductor, they transfer energy to bound valence electrons, generating free electron-hole-pairs, which drift to nearby electrode beads due to the electrical field within the semiconductor. At the electrodes a current can be measured, which is proportional to the energy deposited by the X-rays (Beutel et al., 2000).

3.1.3 Detector properties

Regardless of application, a perfect detector should fulfill two essential characteristics. First, every X-ray photon hitting the detector surface should create a signal. Since X-rays can pass matter, what makes them usefull after all, they also can pass the detector without being detected. The fraction of detected photons N_d to photons hitting the detector N_0 is not exceeding 1 and is called the detection efficiency η_{det}.

$$\eta_{\text{det}} = \frac{N_d}{N_0} \leq 1 \tag{4}$$

Especially at high photon energies, the efficiency can be quite low, so the measurement time must be increased for obtaining low-noise images. The efficiency depends on the choice of the sensor material, but mainly on the thickness of the sensor layer. Since X-ray intensity decreases exponentially with the path length in material, increasing the sensor thickness can significantly improve the detection efficiency.

The second important characteristic for spatial resolving detection systems is the ability to determine the location where an X-ray photon hits the detector surface. In the best case, X-rays are not only detected efficiently, they rather should be detected exactly where the initial interaction took place. Unfortunately, this is usually not the case. When X-rays are absorbed by a material, their kinetic energy is transferred to one or more electrons. These electrons propagate through the medium while transferring parts of their kinetic energy to other electrons until stopped. The path length of electrons in matter can reach some tens of microns. Therefore the signal is blurred over a certain volume. Another effect can cause a longer range, but less intense signal blurring. X-rays are not always absorbed by matter, they can also be scattered, transferring only a part of their energy at the location of their initial interaction, what is called Compton scattering. The scattered photon with the remaining energy can be absorbed in a detector volume quite far away (up to some centimeters) from their first point of interaction, causing two or even more signal spots. These two effects occur in both detector types and can be calculated very well by ROSI. They depend on the layer composition (materials and thicknesses) of the detector. In scintillator based detectors there is one more effect that dominates the signal blurring. When X-rays are converted to visual light in the scinitllation layer, this light is emitted isotropically to all directions. To be detected, it

has to reach the photo diode layer, where it can be spread over some pixels. This blurring scales highly with the distance from the point of light generation to the photo diode layer. Therefore thick scintillators, where light can be produced quite far away from the photo diode layer often yield a poor spatial resolution. The principle is shown in 9. Signals are clearer distinguishable with thin scintillators, but the efficiency is reduced. Every application demands a different trade-off between efficiency and spatial resolution. The generation, absorption and propagation of visible light in media and on material borders can be described by DETECT2000 (G. McDonald et al., 2000), also a Monte-Carlo simulation code.

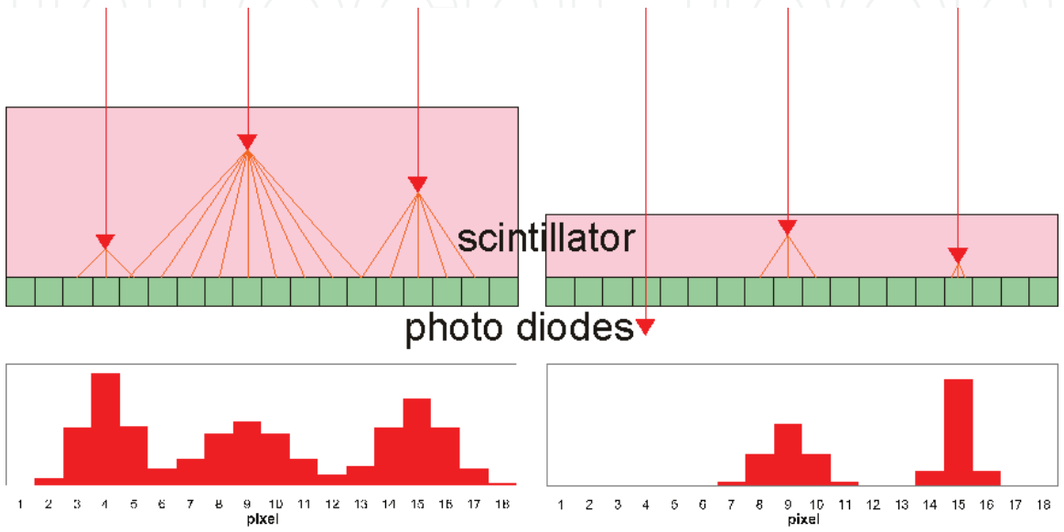

Fig. 9. Signal blurring in a scintillator based detector due to spread of visual photons

For evaluating the relation between the detector properties and their layer composition, one direct converting and one indirect converting detector with 100 μm pixel pitch each were modelled with layer compositions shown in 1.

Detector type	Direct converting (DIC)	Indirect converting (IDC)
Layer composition:		
Front cover	100 μm Al	1 mm Al
Gap	1 mm	1 mm
Front electrode	5 μm Al	
Sensor	750 μm $CdTe$ semiconductor	140 μm Gd_2O_2S scintillator
Rear electrodes	50 μm solder	
Fiberoptic plate		3 mm Al_2O_3
Electronics	1.5 mm Si	1.5 mm Si
Gap	10 mm	
Rear shielding	2 mm steel	400 μm Cu

Table 1. Detector layer compositions

3.2 Simulation of detector properties

3.2.1 Spatial resolution

Like X-ray sources, detectors can be used for a vast amount of applications that demand entirely different properties. Most applications require a good spatial resolution, at least to resolve all details that have to be seen during an inspection. In the last section some effects were introduced that can affect the spatial resolution. The division of the detector in several pixels and their size of course is the most important parameter, but it is mere a numerical issue. The effective spatial resolution can be tested with a double wire test specimen according to the european norm EN462-5. The specimen consists of several pairs of platinum wires with different diameters ranging from 50 to 800 microns. The diameter of each wire of a pair is also the distance between them. This test pattern is placed right in front of the detector entrance window to avoid blurring due to the focal spot. It is also rotated by about 3 degrees to avoid aliasing artifacts. The basic spatial resolution (BSR) can then be derived from the intensity profile perpendicular to the wires. For NDT imaging, the BSR is defined as the theoretical diameter and distance of a wire pair, when the contrast of the space between the wires is at least 20%. To calculate this value, the contrast C_{high} of the wire pair with more than 20% contrast (diameter d_{high}) and the contrast C_{low} of the wire pair below 20% contrast (diameter d_{low}) is determined. The theoretical diameter d_{BSR} of a wire pair with exactly 20% contrast is calculated using linear interpolation.

$$d_{\text{BSR}} = \frac{20\% - C_{\text{low}}}{C_{\text{high}} - C_{\text{low}}} \cdot \left(d_{\text{high}} - d_{\text{low}} \right) + d_{\text{low}} \tag{5}$$

The method is also illustrated in 10. The contrast is calculated from the signal differences $C_{\text{high}} = S_{\text{space,high}}/S_{\text{wire,high}}$ and $C_{\text{low}} = S_{\text{space,low}}/S_{\text{wire,low}}$. The BSR is often given as a spatial frequency in line pairs per millimeter.

$$f_{\text{BSR}} = \frac{1}{2 \cdot d_{\text{BSR}}} \tag{6}$$

Another magnitude often used by detector manufacturers is the modulation transfer function (MTF). Is is usually measured placing a high absorbing plate in front of the detector with a very sharp and straight edge. The intensity profile perpendicular to the edge is called the edge spread function (ESF), differentiating it results in the line spread function (LSF). The MTF is obtained with fourier transformation of the LSF.

$$MTF(\nu) = \frac{1}{\sqrt{2\pi}} \int LSF(x) e^{-i2\pi\nu x} \mathrm{d}x = \frac{1}{\sqrt{2\pi}} \int \frac{\mathrm{d}ESF(x)}{\mathrm{d}x} e^{-i2\pi\nu x} \mathrm{d}x \tag{7}$$

The MTF expresses the contrast transfer of a periodic pattern in dependence of the spatial frequency. For ideal pixel detectors without blurring, the MTF becomes a sinc function, where p is the pixel pitch of the detector.

$$MTF_{\text{ideal}}(\nu) = \frac{\sin\left(2p\pi\nu\right)}{2p\pi\nu} = \operatorname{sinc}\left(2p\pi\nu\right) \tag{8}$$

The upper threshold frequency where periodic structures can be reconstructed with any accuracy is called the Nyquist frequency $\nu_{\text{Nyquist}} = 1/2p$. As with the BSR, it is assumed that a structure can be resolved at a frequency with at least 20% of contrast transfer.

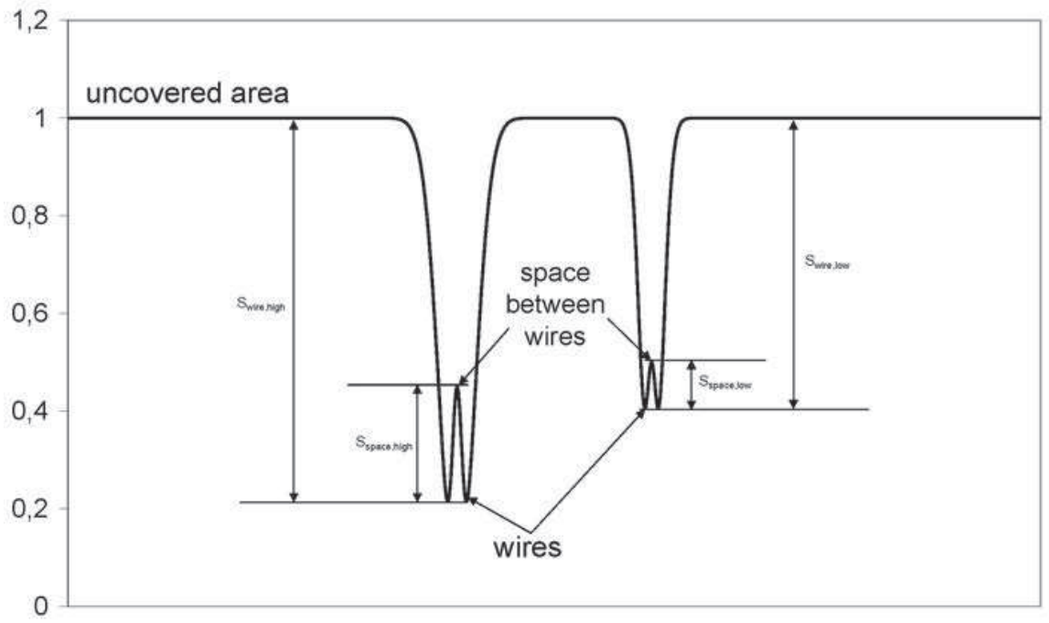

Fig. 10. Method for determining the BSR using the intensity profile along the BSR462-5 double wire specimen

3.2.1.1 BSR test results

BSR images were obtained using the following simulation parameters:

- X-ray source: 3 different voltage, prefilter and focal spot size combinations
  - 30 kV, no prefilter, 2 μm focal spot size
  - 160 kV, 4 mm aluminium prefilter, 300 μm focal spot size
  - 450 kV, 4 mm copper prefilter, 2.5 mm focal spot size
- Distance from source to detector: 1 m
- Irradiated detector area: 102.4 mm x 25.6 mm (1024x256 pixels)
- Object placed directly in front of the detector with a rotation of 3 degrees
- Number of simulated photons per image: 10^9 ($\sim$ 4000 per pixel)

The images taken with both detectors are shown in 11. The blurring due to optical photon scattering in the image taken with the IDC detector can clearly be seen, the DIC image is quite sharper. The resulting BSR values are shown in 2. In the DIC detector, the signal blurring originates from X-ray photon scattering in the detector volume. Since the scattering cross section increases with photon energy, the BSR values also increase with the mean spectrum energy. In the IDC detector, signal blurring is dominated by scattering of optical photons. The mean interaction depth of photons increases with photon energy, so interactions occur closer to the photo diode matrix. The result is a better resolution with higher energies in contrast to DIC detectors.

3.2.1.2 MTF determination

For obtaining MTF images, almost the same parameters were used as for BSR images. To save simulation time, a smaller area of only 12.8 mm x 12.8 mm (128x128 pixels) was irradiated

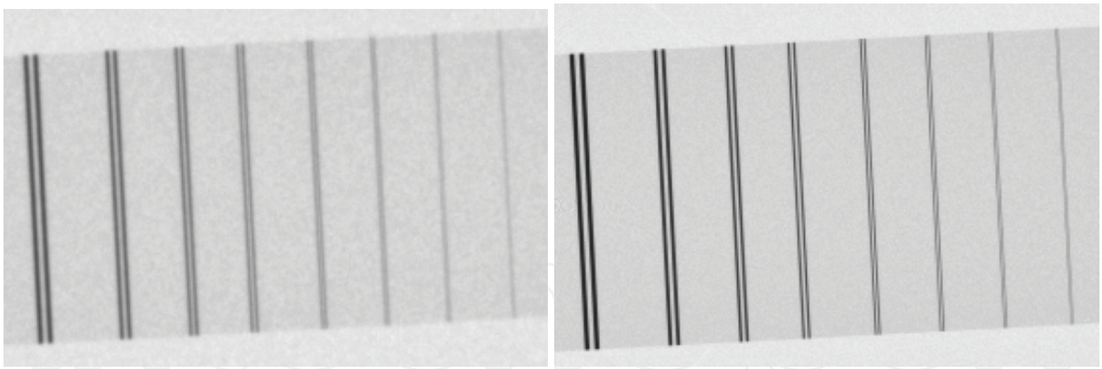

(a) IDC (b) DIC

Fig. 11. Images of EN462-5 double wire test pattern

	Direct converting (DIC)		Indirect converting (IDC)	
Spectrum	BSR / μm	freq. / lp/mm	BSR / μm	freq. / lp/mm
30 kV, no filter	96	5.2	121	4.1
160 kV, 4 mm Al	102	4.9	119	4.2
450 kV, 4 mm Cu	106	4.7	115	4.3

Table 2. BSR values

using 6.25×10^7 photons per image. The test object was a 5 mm thick tungsten plate which was also placed directly in front of the detector and rotated by 3 degrees. The edge of the plate leads through the center of the detector (12).

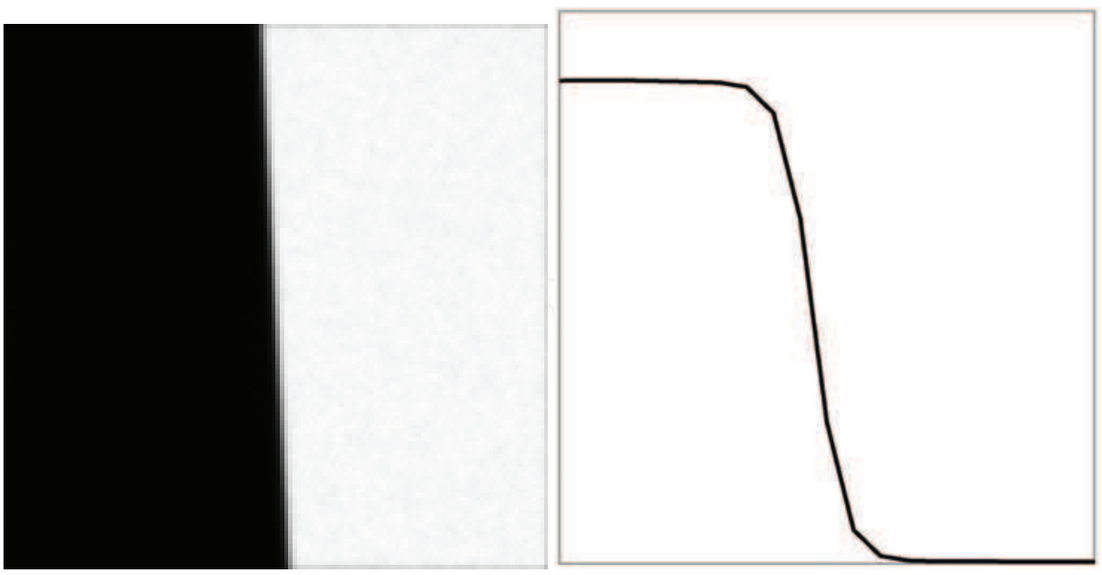

(a) MTF image (b) Edge spread function (ESF)

Fig. 12. MTF image and edge spread function taken with IDC detector at 30 kV

Figure 13 shows the calculated MTFs of both detectors. The DIC detector performs better, especially at higher frequencies where optical photon scattering has the largest influence. At

low frequencies on the other hand, the long ranged X-ray scattering processes dominate. The MTF drops quickly at high energies at the beginning of the MTF curve (low frequency drop).

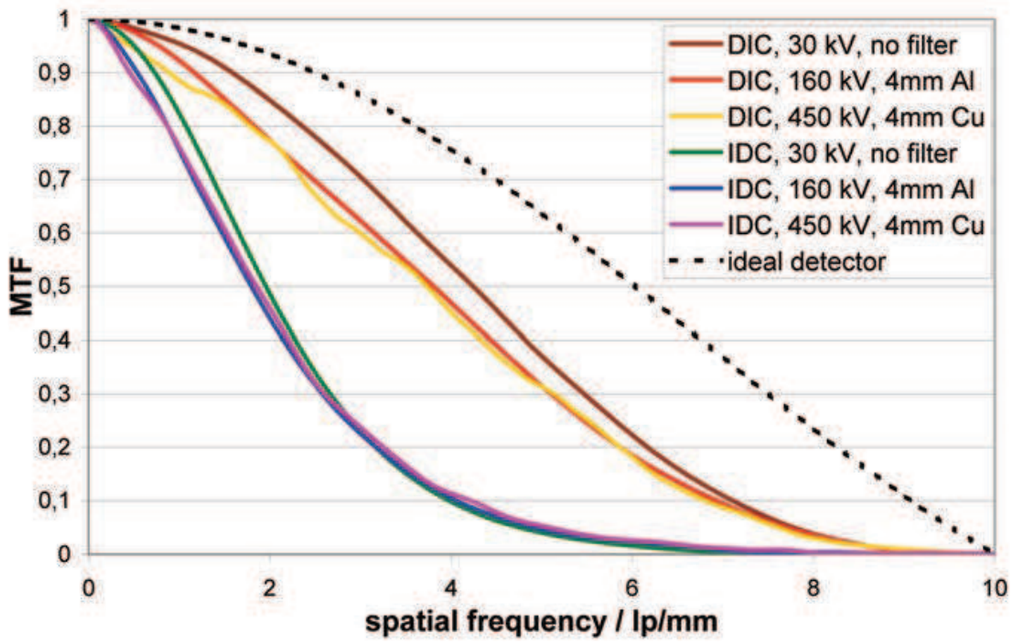

Fig. 13. MTFs for both detectors

3.2.2 Efficiency

The efficiency is the increase of the signal-to-noise-ratio (SNR) in a homogenous irradiated image with the radiation dose. The SNR is the mean signal level of the whole image divided by the standard deviation (the noise). The dose is usually measured as an air kerma value, which is the energy deposition in air per air mass. It is measured in Gray (Gy), 1 Gy = 1 J/kg. Table 3 shows the efficiencies of both detectors. The IDC detector shows higher values, since more blurring lowers the pixel variation of signals. At high energies, the DIC detector gets better, because its the sensor layer is very thick (750 μm) compared to that if the IDC detector (140 μm), so high energy photons can still be detected with a fair efficiency.

	Direct converting (DIC)	Indirect converting (IDC)
	SNR / $\sqrt{\text{Dose}}$	
Spectrum	$1/\sqrt{\text{Gy}}$	
30 kV, no filter	3.76	5.09
160 kV, 4 mm Al	29.0	31.6
450 kV, 4 mm Cu	23.5	22.5

Table 3. Efficiency values

4. Applications

As already mentioned in the previous section, X-ray Monte-Carlo simulation is a very powerful tool for the design, optimization and the ability to evaluate the proof of concept

of complete X-ray non-destructive-testing (NDT) devices. For X-ray imaging devices e.g. the complete life cycle of each single particle (X-ray photon) including all secondary particles (secondary electrons) can be simulated in detail if needed. The accelerated electrons hitting the tube target emitting bremsstrahlung and characteristic radiation depending on the thickness and layer materials of the target. The generated X-ray photons travel to the specimen and interact via Compton scattering or photoelectric effect. Behind the object the interactions of the photons when hitting the detector can also be studied in detail with all occuring effects like distribution of deposited energy in the detector due to X-ray scattering and the range of the secondary electrons (photo electron).

X-ray system design for the inspection of not yet common specimen, whereupon not yet common means, new in object size, new in material or material combination, new in aspect ratio or also new in the task is sometimes challenging, specially if the specimen and the parameters for X-ray imaging can not be directly derived from former measurements of known objects or the predicted hardware for the inspection system is not available.

Subject to the task inspection systems for non-destructive-testing applications can have different geometries resulting in different requirements for its geometry and used components. A complete overview of X-ray NDT systems and its applications would be go too far but the commonly used principles to mention are radioscopy, computed tomography (CT) and X-ray fluorescence methods.

Independent of the method, the same questions are always of interest when a new inspection system is to be evaluated. Most of interest are boundary conditions like the measurement time or the throughput, the possibility of detection of imperfections or the expected pureness of the separation of the bulk material. The answers are often dependent on each other and the challenge is not only if the task is likely to be solved, but also with what quality at what speed. Therefore derived from the task the system has to be designed in virtual reality and virtual optimizations of the setup have to be done with Monte-Carlo simulations. With the help of simulations the expected performance of the planned system can be predicted.

4.1 Radioscopy

In radioscopy each specimen is projected on a detector resulting in a 2D image representing the X-ray absorption coefficient of the penetrated material along the X-ray path through the object. With this technique e.g. aluminum casting parts for automotive industry can be inspected and analyzed for defects which might result in a failure of the part during operation. For safety reasons each part in the production line has to be inspected which leads to a need of a very high throughput. The challenge is always to find an optimal trade-off between high throughput and high image quality. The higher the throughput the lower the image quality due to statistical reasons and the lower the performance of the automated image analysis software of the inspection system.

A lot of effects affect the image quality in radioscopy systems. By optimizing the throughput of the inspection system it is of essential interest to suppress all effects reducing the image quality. One effect e.g. is the scattered X-ray radiation from inside the specimen during inspection which hits the detector and reduces the contrast and sharpness of the projection. This effect leads to reduced possibility of detection of small defects. With the Monte-Carlo simulation is it possible to simulate the scattering effects in the specimen and also the distribution of the scattered radiation on the detector. If we know the intensity distribution of the scattered radiation from the specimen on the detector, it can be subtracted from the real image taken during the inspection. With this operation it is possible to get images of the

specimen with nearly no intensity of scattered radiation resulting in better contrast and higher sharpness of the image. In 14 the simulated projection of a step wegde and the simulated intensity distribution of the scattered radiation is shown. Simulation is the only way to get a realistic and not approximated intensity distribution of scattered radiation.

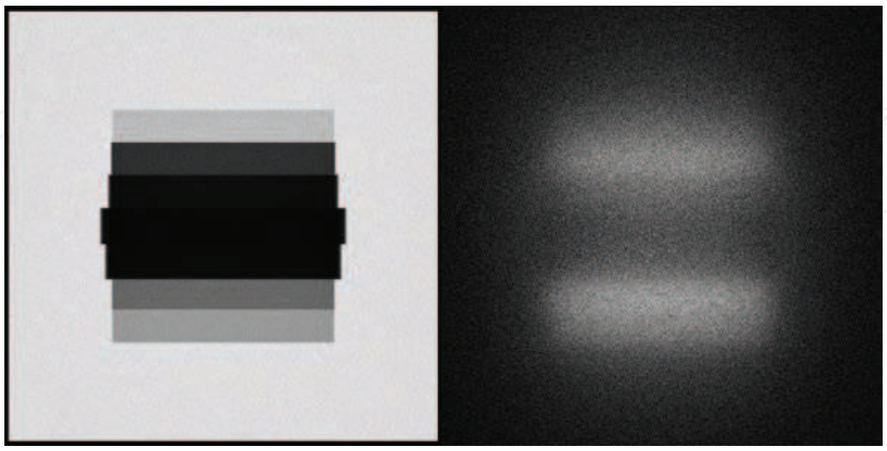

Fig. 14. From left to right: simulated projection of a stepwedge, scattered radiation on the detector.

4.2 Computed tomography (CT)

With computed tomography a 3D distribution of the absorption coefficients of the specimen can be generated providing complete 3D information about the object. The specimen is X-ray projected like many radioscopic images from different angles and the projections can be reconstructed to a 3D volume dataset of the object which can be analysed in 3D.
State of the art e.g. in cargo scanning systems for airport security and customs purposes are 2D scanners providing the personnel only with 2D projections of the freight containers. Due to the overlay projection of different objects in the container the objects often cannot be clearly separated. Driven by this lack of information the idea is to evaluate if it is possible to make a complete CT of the freight container to get the real 3D information. The experimental setup of such a CT system would lead to an investment of expensive equipment. The other way is to virtually design and setup an air cargo scanning system in the Monte-Carlo simulation tool with parameters of real components and make the evaluation with simulations. The virtual setup can be seen in 15.
With this virtual setup in the Monte-Carlo simulation it is possible to predict the expected image quality and recognizability of different materials and objects in an air cargo container together with the scanning times to be expected. In 16 the results of the simulation are shown as reconstructed slices of the air cargo container and its content.

4.3 X-ray fluorescence analysis (XRF)

For the separation of all kinds of bulk material X-ray transmission or X-ray fluorescence methods in combination with a band-conveyor could be a possible solution. Also here is the question at what speed, with what purity and with what spatial resolution the bulk material can be separated. With the Monte-Carlo simulation tool it is possible to simulate the complete process beginning with the optimization of the excitation spectrum, over the excitation of the bulk material with the energy distribution and detection of the excited

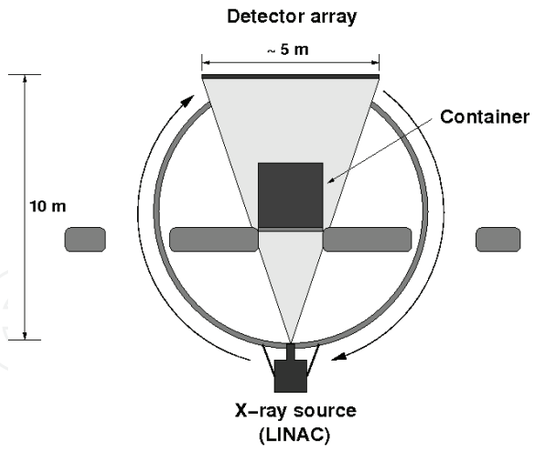

Fig. 15. Sketch of the CT simulation setup of an air cargo container with a LINAC as X-ray source and a 5 m detector array rotating around the container.

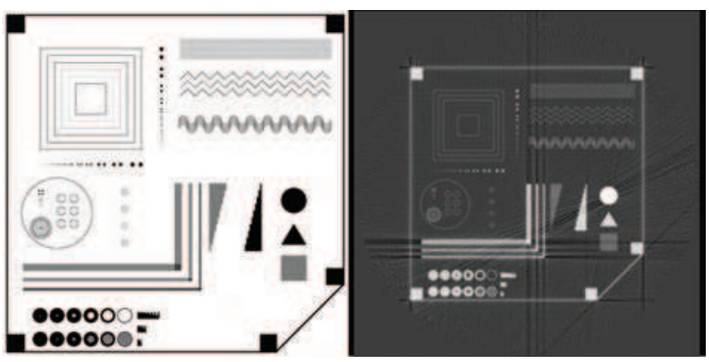

Fig. 16. Left side: One slice of the air cargo container and its content (ideal simulation). Right side: Reconstructed slice of the air cargo container based on simulated projections with reconstruction artifacts due to beam hardening and scattered radiation.

spectrum as a function of different parameters like geometry or X-ray energy. In virtual reality a lot of different parameters in energy, detector systems and geometries can be simulated and evaluated without any real experimental setup. The virtual setup is shown in 17. The simulated detected spectrum of our detector system is shown in 18.

4.4 Dosimetry

Radiation damage due to inspection of some specimen is sometimes a question. For example the dose applied to the content of freight containers or to the electronic parts in PCB inspection systems is of interest to obviate radiation damage and therefore malfunction of the goods. In the MC-Simulation all objects can be defined as detectors which sum up the deposited energy due to the radiation interactions. With summing up the deposited energy it is possible to directly recalculate the applied dose to the specimen in the virtual inspection. With such calculations it is possible to evaluate and predict the applied dose to goods in freight containers which could be expected with a planned inspection system before the system is set up.

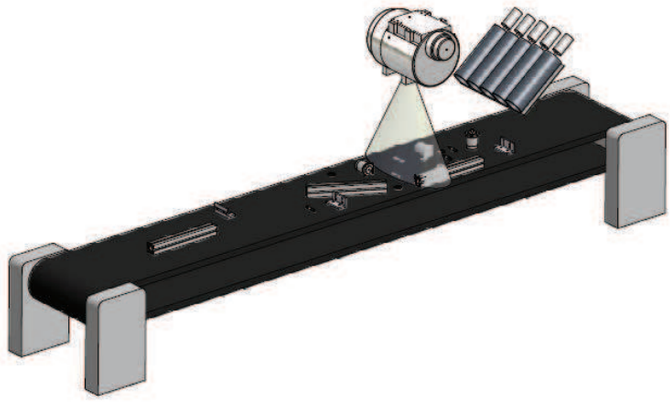

Fig. 17. Setup of the virtual XRF system for evaluation of the expected performance. The high power tube is located above the band-conveyor and to the right of the tube the XRF detector system is located.

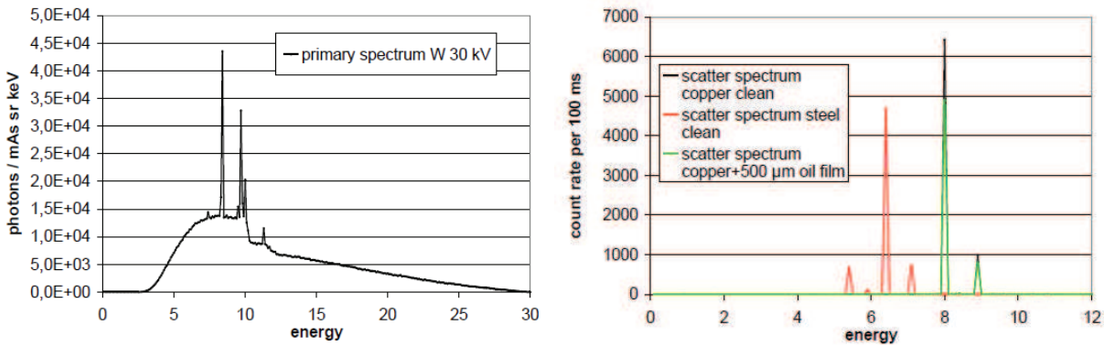

(a) Excitation spectrum (b) Excitated spectrum

Fig. 18. Simulated excitation spectrum and the resulting excitated spectrum of a copper specimen.

5. Conclusion

With the X-ray Monte-Carlo simulation ROSI many scenarios can be modelled and calculated realistically. These reach from X-ray generation over imaging applications to X-ray detection. ROSI has also some limitations, since it assumes that electrons and photons have solely particle character. If effects are based on their wave character, another approach has to be done to describe these effects. The simulation of optical light propagation with DETECT2000 is a good example how several simulation codes can be combited to achieve excellent results. Heat generation in X-ray targets and cooling mechanisms can't be dscribed by ROSI directly. But the simulation can provide valuable data for other simulations like finite element programs, where dynamic heat transfer processes can be calculated from 3-dimensional heat energy distributions over the target volume.
Many studies are already done with ROSI to design X-ray targets, detector or whole X-ray devices. The development of ROSI still goes on to include more detailed effects and simulation possibilities.

6. References

Nelson W.R.; Rogers D.W.O. & Hirayama H. (1985). The EGS4 Code System, *Stanford Linear Accelerator Report SLAC-265*, Stanford, CA 94305

S. Agostinelli et al. (2003). Geant4 - A Simulation toolkit, *Nuclear Instruments and Methods A 506*, pp. 250-303

H. Morneburg (1995). Bildgebende Systeme für die Medizinische Diagnostik, *SIEMENS Publicis MCD Verlag*, ISBN 978-3895780028

J. Beutel; H.L. Kundel & R.L. Van Metter (2000). Handbook of Medical Imaging, Volume 1, *SPIE Press*, Bellington, Washington, USA, ISBN 0-8194-3621-6

J. Giersch & A. Weidemann (2003). ROSI: An object-oriented and parallel computing Monte-Carlo simulation for X-ray imaging, *Nuclear Instruments and Methods A 509*, pp. 151-156

F. Sukowski (2007). Entwicklung von Hochleistungsröntgenröhren mit Hilfe von Monte-Carlo-Simulationen, *Dissertation*, Friedrich-Alexander-University of Erlangen-Nuremberg, Erlangen

J.D. Jackson. Klassische Elektrodynamik (2006), *de Gruyter*, ISBN 978-3110189704

G. McDonald; C. Moisan; F. Cayounet. DETECT2000 the object-oriented version of DETECT, Laval University, Quebec City

Applications of Monte Carlo Method in Science and Engineering
Edited by Prof. Shaul Mordechai

ISBN 978-953-307-691-1
Hard cover, 950 pages
Publisher InTech
Published online 28, February, 2011
Published in print edition February, 2011

In this book, Applications of Monte Carlo Method in Science and Engineering, we further expose the broad range of applications of Monte Carlo simulation in the fields of Quantum Physics, Statistical Physics, Reliability, Medical Physics, Polycrystalline Materials, Ising Model, Chemistry, Agriculture, Food Processing, X-ray Imaging, Electron Dynamics in Doped Semiconductors, Metallurgy, Remote Sensing and much more diverse topics. The book chapters included in this volume clearly reflect the current scientific importance of Monte Carlo techniques in various fields of research.

InTech Europe
University Campus STeP Ri
Slavka Krautzeka 83/A
51000 Rijeka, Croatia
Phone: +385 (51) 770 447
Fax: +385 (51) 686 166
www.intechopen.com

InTech China
Unit 405, Office Block, Hotel Equatorial Shanghai
No.65, Yan An Road (West), Shanghai, 200040, China
中国上海市延安西路65号上海国际贵都大饭店办公楼405单元
Phone: +86-21-62489820
Fax: +86-21-62489821

IntechOpen